
MULTISCIA
JOURNALS PUBLISHERS
FRONTIERS IN CLINICAL TRIALS AND DRUG INTERACTIONS
ISSN: (3065-3975)
https://multisciajournals.com/journals/index.php/fctdi
editor.fctdi@gmail.com

Frontiers in Clinical Trials and Drug Interactions
Volume1, Issue2, 2025

Remotely Activated Scaffolds for Managed Drug Release

D Vishnyakova

Department of Clinical Trials and Drug Interactions

Article Info

Received: 25-03-2025 ***Revised:22-04-2025*** ***Accepted:07-05-2025*** ***Published:17-05-2025***

Abstract: Fe3O4-Au hybrid nanoparticles (HNPs) have shown growing promise for biomedical uses, including medication delivery that responds to image-guided stimuli. Future biological applications might greatly benefit from incorporating the special qualities of HNPs into thermally sensitive scaffolds. Here, we effectively created thermoresponsive poly(N-isopropylacrylamide) (pNiPAM)-based smart scaffolds. When exposed to a brief laser burst, nanoparticles that provide a localized heating trigger were discovered to enable remote control of bulk polymer shrinkage. Wet chemical precipitation techniques were used to create gold-covered iron oxide nanoparticles, which were then electrochemically coated. Following the functionalization of the particles with allyl methyl sulfide, mercaptodecane, cysteamine, and poly(ethylene glycol) thiol to improve stability, live/dead staining and cell membrane integrity investigations using lactate dehydrogenase (LDH) quantification were used to determine the precise biological safety. After being exposed to 7F2 cells, the PEG-coated HNPs did not exhibit a significant cytotoxic impact or bad cellular response ($p < 0.05$), therefore they were continued for scaffold integration. A Q-switched Nd:YAG laser was used to examine the pNiPAM-HNP composite scaffolds' potential as thermally triggered systems. These experiments demonstrate that the addition of HNPs caused internal structural heating, which led to scaffold deformation after extremely brief irradiation durations (seconds). Using methylene blue as a model drug that is released after remote structural modification of the scaffold, our studies demonstrate the potential of these hybrid-scaffold structures for use in drug delivery.

Keywords: scaffold; smart material; thermo-responsive; hybrid nanoparticle; surface plasmon

1. Introduction

New materials for use in implant technology [1], in vitro cell growth for regenerative medicine [2], and medical diagnostics [3] have been developed as a result of advances in our understanding of cell-material interactions. To enable the flow of nutrients and toxins to developing tissue, scaffolds used for tissue engineering applications must have regulated pore sizes [5] and structures [4] [6]. For cells to grow into a three-dimensional structure, the right conditions must be present. Although scaffold materials often present issues for long-term regeneration, they provide the architecture to facilitate 3D tissue formation [7]. For long-term applications, such as supporting tissue formation or serving as delayed drug release carriers, biodegradable scaffolds that decompose after a certain amount of time—either spontaneously or in response to an external stimulus—are beneficial [8]. When nanoparticles are included into a scaffold's natural structure, they may improve functioning and provide intriguing new features like the capacity to remotely cause structural collapse, which may eventually result in drug release. The potential of gold-coated iron oxide hybrid nanoparticles (HNPs) for use in biomedicine is growing [9–11]. These hybrids are easily fabricated, yielding particles with consistent physicochemical characteristics and size [10]. The iron oxide core may be used as a contrast agent in magnetic resonance imaging (MRI) [13] or for external guiding [8,12]. Surface plasmon properties are present in the inflexible gold coating [14]. When certain particles are exposed to light, this process causes light to quickly transform into thermal energy [15]. The "biological window," where light is strongly transmitted through tissues yet may provide a mechanism of distant temperature switching, is where it is important to create particles with appropriate absorption

wavelengths [14]. This range is 750–850 nm [15]. When these nanoparticles are incorporated onto a biocompatible scaffold, a more complex system with greater tissue engineering capability is produced. Here, the scaffold's three-dimensional structure may be deformed by taking advantage of the heating of the particles caused by laser irradiation. Finally, the scaffold holes may be modified to contain growth factors or medication molecules, which could then be thermally released into the surrounding tissues. The creation of such a system would enable the targeted release of bioactive compounds and provide a framework for tissue engineering that degrades thermally. The cores of the dense nanoparticles will also provide contrast in MRI images, which may be utilized to see and track the location and deterioration of scaffolds.

At its lower critical solution temperature (LCST), the thermally modified polymer poly(N-isopropylacrylamide) (pNiPAM) undergoes a reversible coil-to-globule conformational shift [16]. When the LCST is surpassed, the polymer forms a dense precipitate in the aquatic environment [17]. Below the LCST, pNiPAM exposes hydrophilic segments to the surrounding aqueous environment, facilitating swelling. About 32 °C is the LCST for pNiPAM [18]. This

2. Results and Discussion

2.1. NiPAM Scaffold Charcteristics

N-Isopropylacrylamide was polymerized to create scaffolds that created a thermoresponsive pNiPAM network. According to the predicted structure of the polymer, the FTIR spectra for pNiPAM (Figure 1) exhibit expected bands at 3500–3200 cm−1, 1600 and 1500 cm−1, and 2800 and 1400 cm−1 originating from the N–H, C=O, and C–H bonding, respectively. When subjected to temperature fluctuations, pNiPAM polymers have a special property that causes the structure above the LCST to collapse due to contact between the polymer chains and an aqueous solvent, hence changing the bulk morphology. Here, the scaffolds were made as monoliths for laser deformation and drug release experiments, or as thin surface coatings (~0.25 mm thick) on glass coverslips for cell culture. By varying the ratio of NiPAM monomer to MBA cross-linker, a variety of gels with varying chain lengths and levels of cross-linking were created (Table 1). In order to create gels with the best control over heat switch deformation while maintaining the capacity to withstand numerous switching cycles, gel elasticity was studied. Immersion in a temperature-controlled water bath set at 25, 30, 40, and 50 degrees Celsius (returning to room temperature in between each cycle) was used to assess swelling characteristics. Repeated heating cycles were used to measure the amount of mass that remained after solvent ejection during shrinkage. Figure 2 illustrates the effects of successive heating and cooling cycles on gel properties. All gels were shown to initially decrease in mass upon solvent ejection when heated, with higher temperatures causing greater degrees of shrinkage for all tested gels. One of the gels showed expansion over its initial cast volume at higher temperatures. For all scaffolds, slight modifications up to around 15% of original mass were seen at 30 °C; as may be predicted, a greater degree of cross-linking was found to limit this change. The biggest change is seen in gels, particularly in their expansion upon heating to 50 °C.

be used for contractile and expansion of a scaffold structure via externally applied heating (and cooling) [27]. Repeated cycles showed that the scaffolds were elastically deforming under these conditions and so would be useful for repeated expulsion of solvent (incorporating drug molecules). Gels could be reduced in volume by heating and remained at this volume if solvent was removed, even upon cooling to 4 °C, Figure 2D. When re-solvated these gels slowly expanded back to their original mass over several minutes.

Figure 1. Representative FTIR spectra of pNiPAM polymer used in scaffold formation, with insert showing chemical structure.

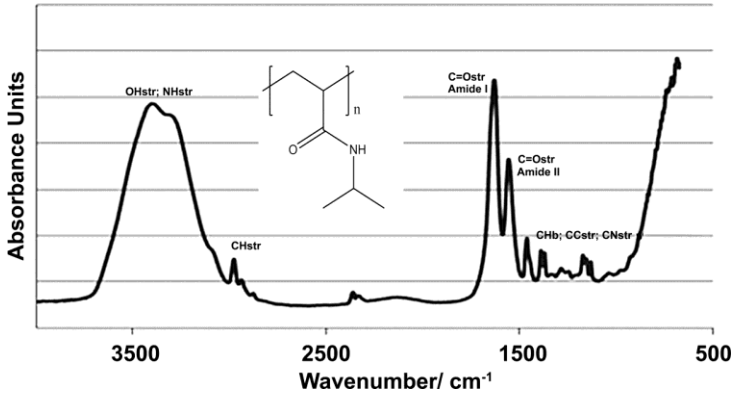

Table 1. Poly(*N*-isopropylacrylamide) (pNiPAM) gel samples investigated using various polymer gel compositions.

Constiutent component	Required amount for 1 mL solvent			
	0.7 M (A)	**0.5M (B)**	**0.3M (C)**	**0.1M (D)**
Water	1 mL	1 mL	1 mL	1 mL
NiPAM	0.0795 g	0.0568 g	0.03408 g	0.01136 g
MBA	1.32 mg	0.943 mg	0.5658 mg	0.1896 mg
APS	0.01 mg	0.01 mg	0.01 mg	0.01 mg
TMEDA	4 µL	4 µL	4 µL	4 µL

Figure 2. Cyclic heating properties of pNiPAM gels at (**a**) 30 °C; (**b**) 40 °C and (**c**) 50 °C. (**d**) Image of gels remaining shrunk when solvent removed after heating and returned to room temperature.

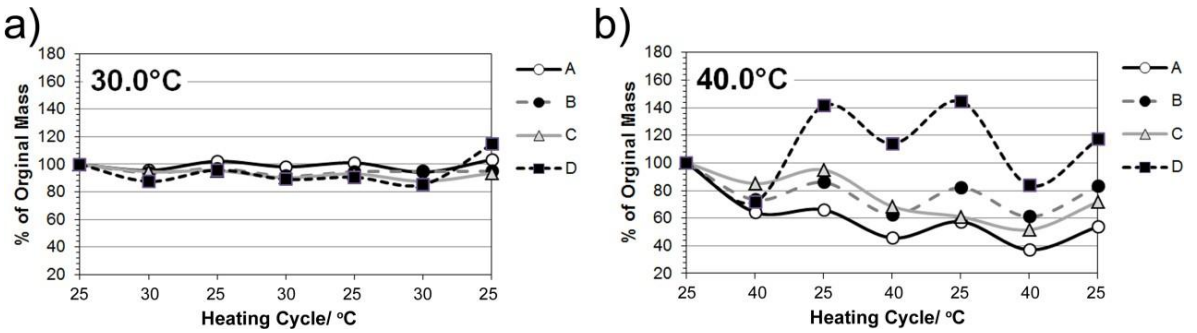

Figure 2. *Cont.*

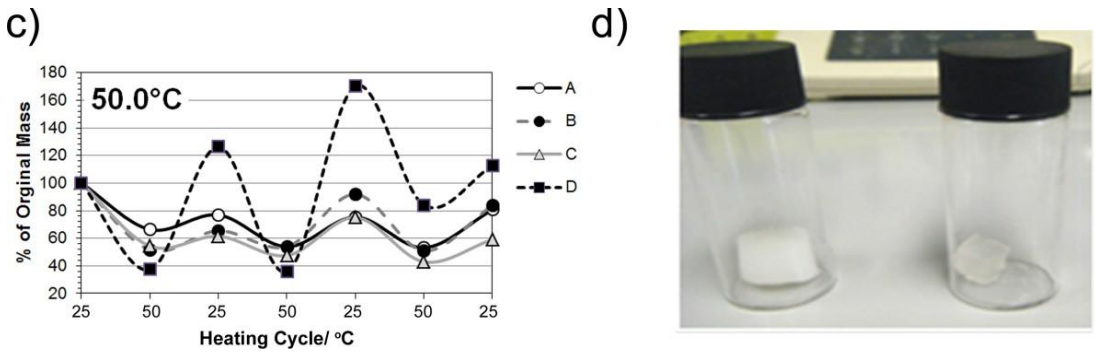

2.2. Synthesis and Characterization of Hybrid Nanoparticles

Iron oxide precipitation followed by electrochemical gold coating was used to create and characterize hybrid nanoparticles. To preserve the intrinsic qualities of the component parts, a polymer intermediate was positioned in between the iron oxide core and the gold covering. The process of seeding and iteratively reducing acidic gold onto the surface of the nanoparticles produced the gold coating. Zeta potential measurements of the particles in water were used to precisely monitor the gold coating process, and inductively coupled plasma–optical emission spectroscopy (ICP-OES) was used to ascertain the metal content (Table 2). Due to the electronegativity of the gold seeds and, eventually, the coat lowering the total surface charge, the zeta potential decreased from the initial +47.4 mV of the PEI coated iron oxide to +10.5 mV when gold coating was attained. The stiff gold coating that formed around the flexible PEI reduced its hydrodynamic diameter and minimized aggregation because of the particles' intrinsic magnetism, which explains why the particle diameter seemed to decrease across the coating phases (Table 2). The TEM image of the gold-coated nanoparticles with an average particle diameter of 70 nm (n = 20, determined using ANALYsis software) is shown in Figure 3a. Additionally, the pictures show that individual iron oxide nanoparticles rather than particle clusters were coated with gold. The hybrid nanoparticles' UV spectroscopy revealed a peak absorption at 690 nm (Figure 3b). The gold shell's plasmon resonance is shown by this wavelength. The peak's existence also suggests that the gold coating was effective since, in the absence of a full coating, the individual gold seeds resonate at around 520 nm. The magnetization vs. applied field hysteresis loop obtained for the samples at 250 K is shown in Figure 4a. Highly crystalline Fe3O4 nanoparticles that are magnetically ordered at ambient temperature are shown by the magnetic coercivity and saturation magnetization values at T = 250 K. Ferromagnetic nanoparticle characteristics may be seen in the zero field cooled/field cooled curve (Figure 4b). The ordering temperature is higher than room temperature, as seen by the lack of a maximum in this data.

In order for these iron oxide-gold coated nanoparticles to become biologically applicable they first require surface engineering with bioactive or biocompatible molecules, polymers or ligands. Hence, the nanoparticles were further functionalized through dative covalent bonding with four thiol or sulfide containing entities including cysteamine, allyl methyl sulphide, poly(ethylene glycol) thiol (PEG-Thiol) and mercaptodecane. The coated nanoparticles were characterized using ICP-OES, zeta potential measurement, photon correlation spectroscopy (Table 2), UV-Vis spectroscopy (Figure 3b) and DRIFT FTIR (Figure 5). FTIR spectra show the presence of aliphatic CH stretching bands associated with the presence of the functional group backbones. After coating the UV peak absorption was further red shifted towards the NIR region (approx. 720 nm). Thus, for optimal thermal effect laser irradiation should be carried out at this wavelength. The coating process for all HNPs was successful, which on visual inspection, could be observed by their greater solution stability compared with their uncoated counterparts.

Table 2. Hybrid nanoparticle characterization using photon correlation spectroscopy, zeta potential measurement and concentration measurements using inductively coupled plasma–optical emission spectroscopy (ICP-OES).

Particle	Metal content analysis ug mL^{-1}		Size nm (±SD)	PDI (±SD)	Zeta potential mV (±SD)
	Fe	Au			
Fe_3O_4	7000	-	2250 (125)	0.540 (0.125)	−16.5 (1)
Fe_3O_4-PEI	1920	-	270 (11)	0.125 (0.004)	+47.4 (3)
Fe_3O_4-PEI-Au_{SEED}	1025	45	190 (9)	0.254 (0.001)	+27.5 (1)
Fe_3O_4-PEI-Au_{COAT} (HNP)	990	370	115(5)	0.258 (0.011)	+10.5 (0)
HNP-Cysteamine	868	323	413 (13)	0.679 (0.082)	+30.4 (1)
HNP-allyl methyl sulfide	885	385	392 (59)	0.738 (0.147)	+39.1 (4)
HNP-PEG	898	377	141.9 (4)	0.321 (0.054)	+20.5 (1)
HNP-mercaptodecane	924	370	442 (21)	0.921 (0.137)	+23.6 (2)

Figure 3. Characterization of hybrid nano-particles. (**a**) Transmission electron microscopy image of nano-particles and (**b**) UV-Vis spectroscopy of nano-particles suspended in deionized water.

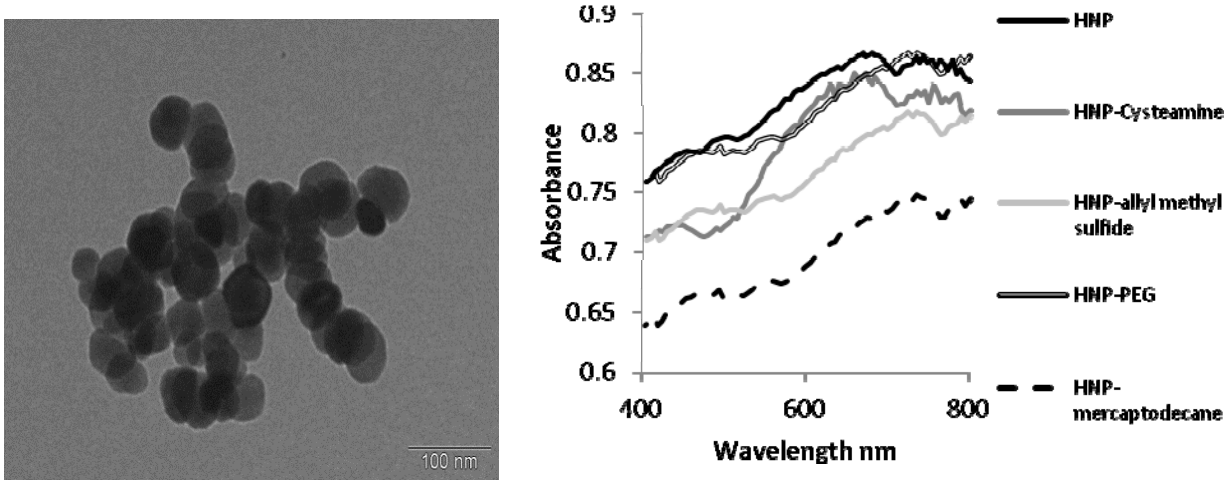

(**a**) (**b**)

Figure 4. Magnetization data of Fe_3O_4-Au hybrid nanoparticles (HNPs). (**a**) M(T) curves measured in zero-field cooled warming and field-cooling mode; (**b**) M(H) curves collected at 250 K between −4 and 4 MA/m and (**c**) M(H) curves measured at 250 K.

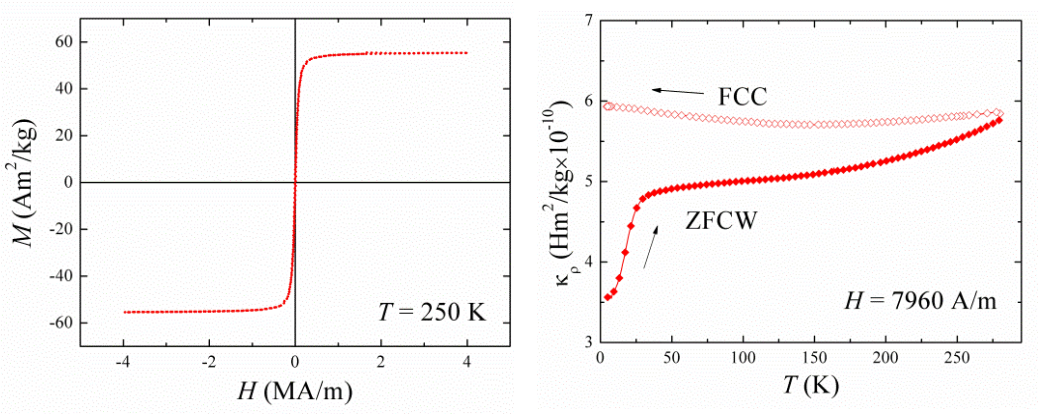

(**a**) (**b**)

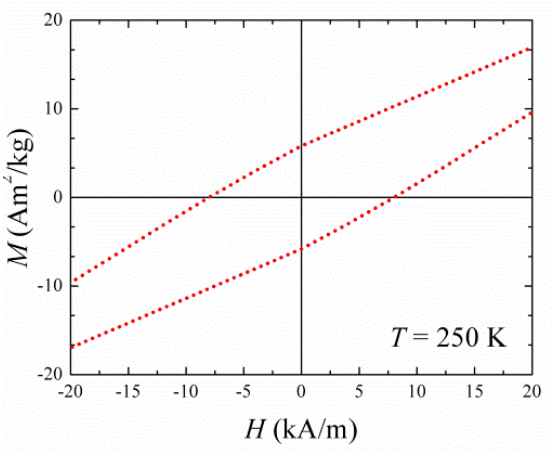

(**c**)

Figure 5. DRIFT FTIR spectra of functionalised hybrid nanoparticles. CH stretch region indicating presence of linker-surface groups.

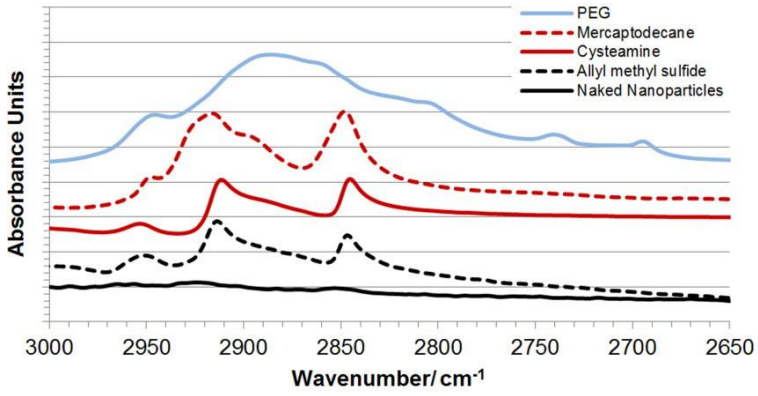

2.3. Biological Characterization of Polymer Coated Hybrid Nanoparticles

Mouse osteoblast (7F2) cells were used in trypan blue exclusion cytotoxicity investigations (Figure 6a–d). According to the findings, PEGylated nanoparticles (HNP-PEG) had the lowest

cytotoxicity on 7F2 cells over the 72-hour testing period, with the maximum incubation dose (100 µg mL−1) showing over 80% cell viability. However, only 40% and 60% of the cells cultured with HNP-cysteamine and HNP-allyl methylsulfide, respectively, were viable after 72 hours at 100 µg mL−1. Following the research period, no live cells were seen following exposure to HNP-mercaptodecane at this concentration. With the abundance of research on PEG's biocompatible qualities [28–31], these results are not surprising. PEG is an FDA-approved polymer that is often utilized in medical device coatings [34], drug delivery [33], and transfection [32]. Therefore, PEG-coated nanoparticles were used in the ensuing tests. According to cellular internalization tests, after only 4 hours, up to 1 pg of HNP-PEG was taken up by the cells, and after 24 hours, that amount rose to 7 pg (Figure 7a). This suggested that the rate of cellular absorption was time-dependent. Lactate dehydrogenase (LDH) quantification was used to examine how exposure to nanoparticles affected the integrity of the cell membrane (Figure 7b). In this case, if exposure to nanoparticles had caused any damage of the cell membrane, LDH levels would have increased. Since there was no extra LDH in the 7F2 control cells when compared to the basal levels, the result indicates that no significant membrane damage had occurred. According to these biological investigations, the HNP-PEG did not cause this cell line to exhibit any negative biological reactions in vitro. Additionally, prior research has shown that HNP-PEG does not cause human pancreatic adenocarcinoma (BxPC-3) and differentiated human monocyte (U937) cells to experience elevated levels of cellular stress brought on by lipid peroxidation and free radical formation via reactive oxygen species [35]. There is no discernible reason why the HNPs would not be suitable for integration into the integrated pNiPAM scaffold structure, given our new results and earlier toxicity research on HNPs [35]. When incorporated into the pNiPAM structure, the scaffold may be laser-manipulated, potentially leading to stimuli-responsive drug release.

Figure 6. Cytotoxicity of polymer coated nano-hybrids on 7F2 cells over □ 24 h and ■ 72 h. Coating with (**a**) cysteamine; (**b**) allyl methyl sulphide; (**c**) PEG and (**d**) mercaptodecane.

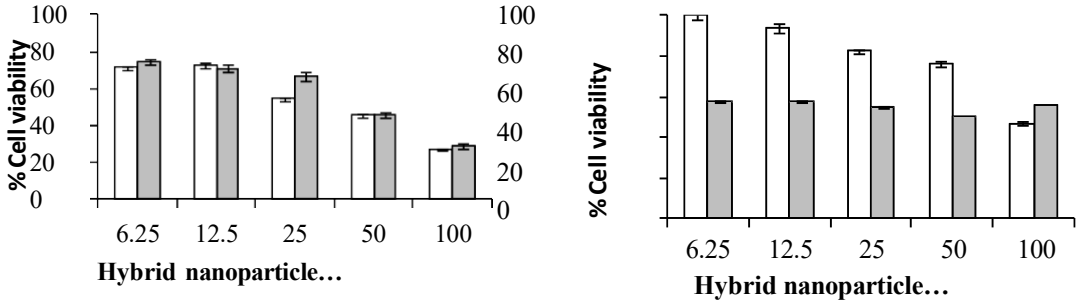

(**a**) (**b**)

Figure 6. *Cont.*

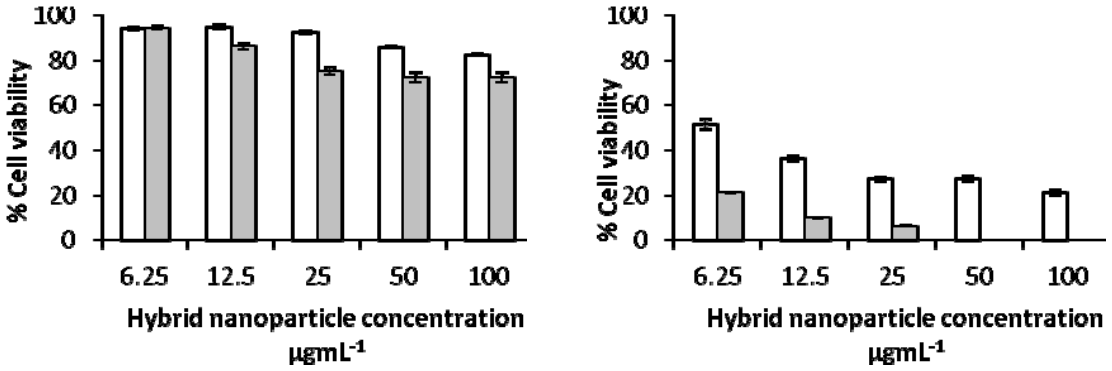

(**c**) (**d**)

Figure 7. Biological investigations of nano-particle exposure in 7F2 cells. (**a**) Cellular uptake of HNP-PEG into 7F2 cells analysed using ICP-OES and (**b**) cell membrane integrity assay measured via lactate dehydrogenase quantification.

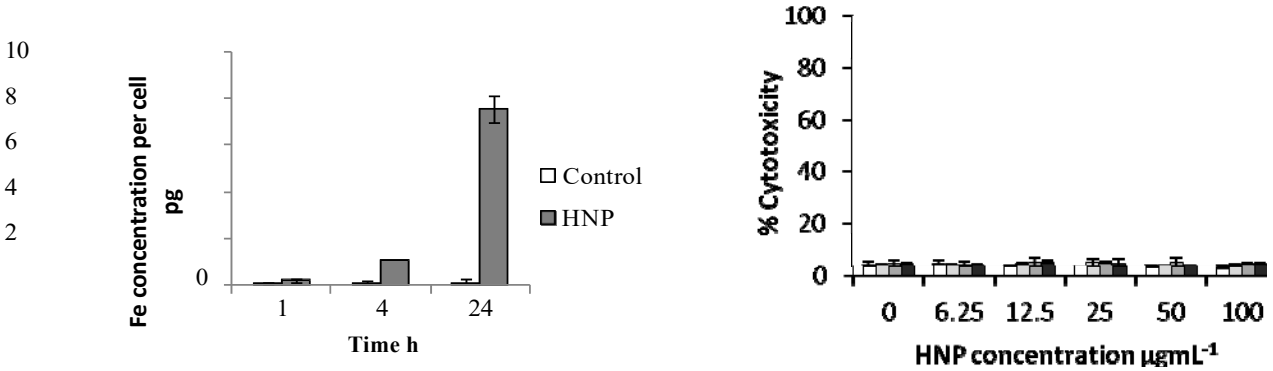

(**a**) (**b**)

2.4. Laser Irradiation of HNP-PEG Phantoms

Laser irradiation was carried out of HNP-PEG suspended in an agar (2%) phantom in 3.5 mm discs. The temperature increase was recorded at both the laser beam focus and in the surrounding sample to determine whether the heating was localized or whether bulk heating occurred (measured using thermocouples). Here, thermal increase was only experienced inside the laser beam diameter (7 mm) and no bulk heating was observed. Figure 8 shows the temperature change occurring when the HNPs were irradiated over 10, 20, 30, 40 and 60 s. The data suggests that the HNPs experienced an irradiation time dependent heating pattern, whereby, after 60 s the greatest temperature change of 25 °C was observed. This large increase in temperature over a short laser exposure time holds great potential for thermal manipulation of biomaterials such as scaffolds. Very minor thermal deviations were observed in the pNiPAM control, Figure 9, indicating the localization of heating effect to the nanoparticles.

Figure 8. Temperature change in HNPs (50 ug mL^{-1}) suspended in an agar phantom exposed to laser irradiation using a Q-switch Nd:Yag laser at 10 pulses s^{-1}. All samples equilibrated to room temperature before beginning. Control sample consisted of 2% agar with no nanoparticles.

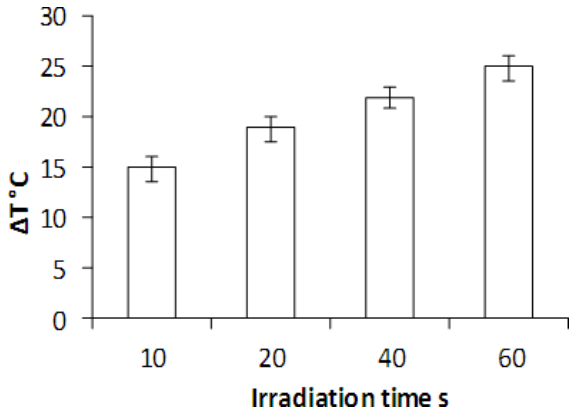

Figure 9. Physical properties of pNiPAM-HNP composite. (**a**) Temperature change in pNiPAM-HNP composite exposed to laser irradiation using a Q-switch Nd:Yag laser at 10 pulses s^{-1}. FESEM images of composite (**b**,**c**).

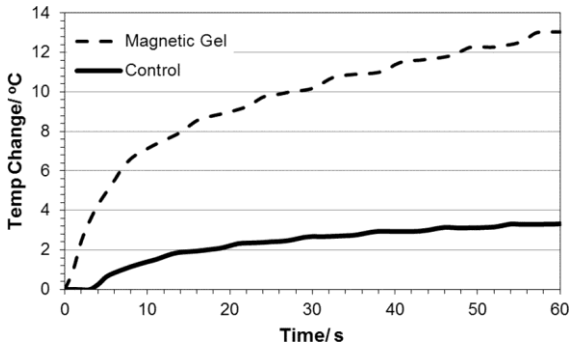

(**a**)

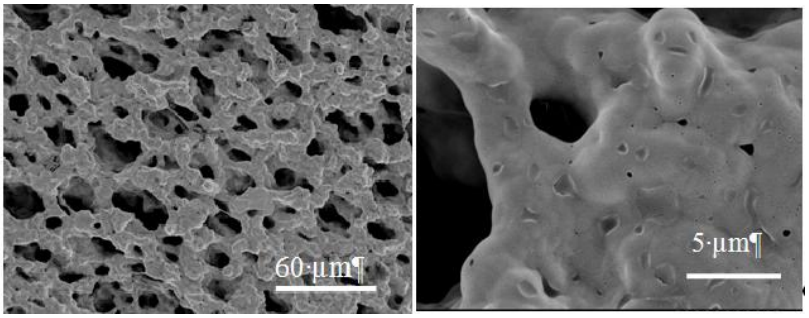

(**b**) (**c**)

In this study we used a nanosecond (Q-switched) pulsed laser fixed at 532 nm. As earlier discussed, a laser of wavelength 720 nm would be more appropriate for application due to the peak plasmon resonance observed after PEGylation, however, the peak absorbance on the UV-Vis spectra (Figure 3) was relatively broad and so heating effects were expected at 532 nm. Hence, these results may be greatly improved upon application of laser irradiation closer to the plasmon resonance wavelength.

2.5. Studies on pNiPAM-HNP Composites

HNPs were successfully incorporated into the intrinsic structure of the scaffolds. This was evident from a color change in the bulk scaffold from a translucent pale white to a grey. Field Emission Scanning Electron Microscopy (FESEM) showed the matrix structure formed (Figure 9a). At increased magnification small nano-sized pores where evident which possibly were due to the HNP penetration into the intrinsic structure upon fabrication (Figure 9c). SEM EDX confirms the presence of HNPs inside the pNiPAM matrix (Figure 10). The pNiPAM-HNP composites were exposed to laser irradiation over 60 s and the temperature change measured using thin wire thermocouples. Figure 9a shows the temperature increase for the nanoparticle containing scaffold at 13 °C over the exposure period. Control scaffolds not containing nanoparticles were observed to heat minimally ~3.5 °C. Only those scaffolds hosting hybrid nanoparticles were distorted by the temperature changes induced by the irradiation, leading to expulsion of previously entrapped solvent out of the polymer network. This ability to manipulate scaffold integrity is thought to be beneficial in controlled drug delivery. Encapsulation of drug into the scaffold pores which could be released upon external stimulus could revolutionize controlled drug delivery. In addition, the inherent magnetism of the HNP core is suitable for MRI guidance; amalgamation of these two properties holds great potential for image guided prolonged drug delivery.

Figure 10. Electron microscopy and related EDX analysis indicating nanoparticle-polymer hybrid scaffolds. (**a**) SEM image; (**b**) iron; (**c**) gold and (**d**) overlaid iron and gold EDXA maps.

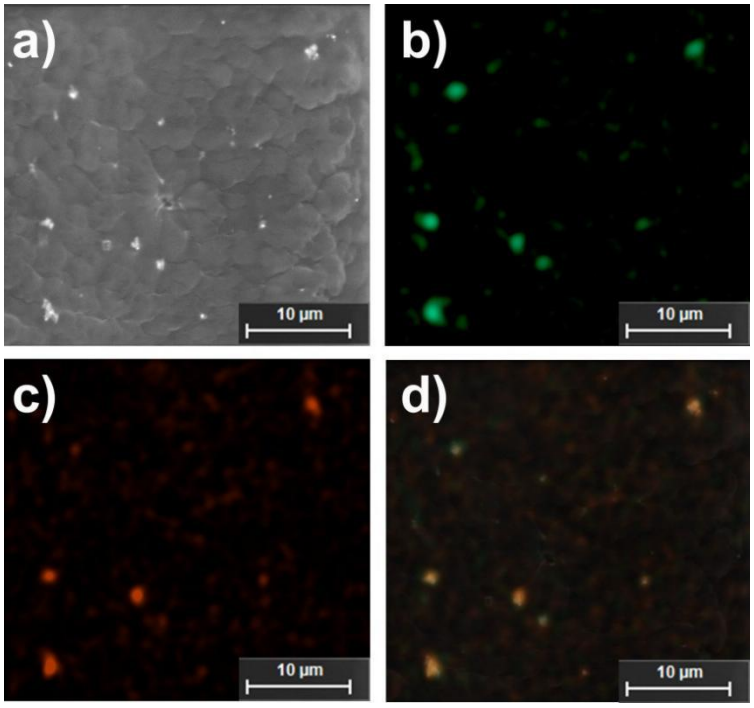

2.6 Stimulated Release of Model Compound

pNiPAM-HNP composites were prepared containing methylene blue (MB) dye as a model drug, chosen for its intense absorption in the UV/Vis range allowing visualization during expulsion from the scaffold after thermal deformation. Gels were prepared either polymerized with dye *in situ* or post

incubated in dye solution. All gels were rinsed thoroughly prior to laser irradiation to remove any surface dye, with one of the scaffolds formed with MB in the mix also left rinsing in dH_2O for 2 days prior to experimentation. Upon laser irradiation samples were again found to deform, expelling solvent carrying MB out of the polymer network. This solution was harvested and assessed for quantification of MB using UV-Vis spectroscopy. Figure 11 shows that less dye was released in the post-incubated scaffolds, however this is probably due to a reduced quantity of dye being incorporated into the pore network through diffusion controlled ingress. Pre-loaded scaffolds have a higher amount of dye within the structure, so upon deformation larger amounts can be released giving rise to higher levels of expelled dye. The same samples were irradiated twice, with a short time in-between to remove any expelled solvent volume. Where pre-loaded samples showed a slight decrease in the amount of dye released during the second irradiation/ deformation, similar levels were observed for scaffolds post-incubated in dye solution. This again may be due to the locality of the dye near to the surface of the gel. These results show clearly the ability to remotely control switching of the hybrid scaffold materials to cause thermal deformation, resulting in release of a model drug compound.

For scaffolds pre-loaded with the dye during polymerization, more dye was released during the first irradiation compared to the second.

Figure 11. Expelled amount of methylene blue during laser irradiation of hybrid scaffolds.

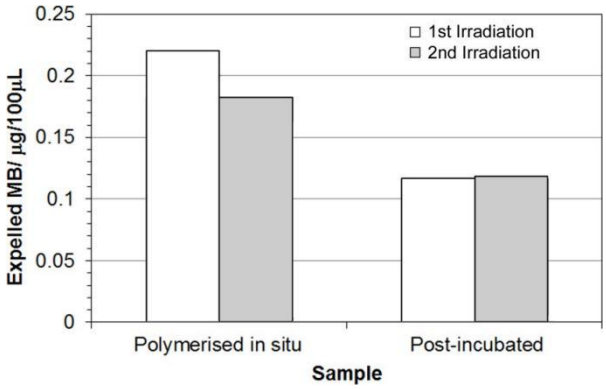

3. Experimental Section

All materials were purchased from Sigma-Aldrich (Dorset, UK) unless otherwise stated.

3.1. Scaffold Formation

The pNiPAM scaffolds were analyzed using Fourier Transform Infrared Spectroscopy (FTIR) in order to characterize bonding structure in the polymer. pNiPAM gels were measured using a single bounce germanium attenuated total reflectance attachment (Nicolette IS50, Thermo-Fisher, Loughborough, UK). The samples were scanned taking an average of 128 spectra. Scaffolds were super critically dried after methanolic exchange, and imaged using scanning electron microscopy (SEM) and energy dispersive X-ray analysis (EDXA).

3.2. Synthesis of HNPs

Iron oxide cores were synthesized using a previously reported precipitation reaction [10,36,37]. Briefly, sodium hydroxide (NaOH, 1.030 g) and potassium nitrate (KNO_3, 1.820 g) in deionized water (H_2O, 180 mL) was refluxed at 90 °C under nitrogen (N_2) for 1 h. Iron (III) sulphate heptahydrate ($Fe_3O_4.7H_2O$, 3.89 g) in sulphuric acid (H_2SO_4, 20 mL) was added to the reaction and heated for 24 h at 90 °C. The black precipitate was cooled on ice and washed in H_2O (six times). The magnetic particles formed were easily separated from solution using a high powered magnet and resuspended in water. A poly(ethylenimine) (PEI) intermediate was added via probe sonication of 5 mL magnetic particles with 5 mg mL^{-1} polymer in deionized water. Gold seeds were electrostatically attached to the polymer followed by reduction of $HAuCl_4$ onto the particle surface forming a complete shell [38]. Hybrid nanoparticles were surface functionalized with cysteamine, allyl methyl sulphide, poly(ethylene glycol) and mercaptodecane via dative covalent bonding between the HNP (5 mg mL^{-1}) and the SH groups in the polymers (5 mg mL^{-1}). The final particles were washed extensively with deionized water to ensure excess polymer was removed before re-suspending in 5 mL deionized water.

3.3. Characterization of HNPs

Metal quantification was determined using inductively coupled plasma-optical emission spectroscopy (ICP-OES, Optima 7000V DV, PerkinElmer, Wokingham, UK). An acid digestion was carried out in concentrated nitric acid (HNO_3, 1:5 sample:acid). The samples were diluted with deionized water prior to analysis. A calibration was run using iron and gold standard solutions 0.5–5 mg mL^{-1} (R = 0.9999). The concentration of HNPs used for all experiments indicates the concentration of Fe. Peak absorbance of HNPs in deionized water was measured using a Varian UV-Vis Cory 50 Bio spectrometer (Agilent, Wokingham, UK). Samples were analyzed in quartz cuvettes, absorbance scans were carried out between 200–800 nm. Polymer coating was determined using FTIR analysis as previously described. Hydrodynamic diameters and polydispersity index were estimated using photon correlation spectroscopy (PCS) (Zetasizer Nano-ZS, Malvern Instruments, Malvern, UK). All measurements were carried out at 25 °C (n = 3) and an average value determined. Zeta potential measurements were carried out to determine surface charge using the same instrument. Transmission electron microscopy (TEM) was used to visualize the particles. Samples were pipetted onto formvar coated copper grids (2 µL) and dried under a heat lamp for 4 h. The grids were directly imaged using a JEOL JEM-1230 microscope with ANAlysis software (JEOL, Japan). Magnetic characterisation was carried out in a Quantum Design MPMS-XL SQUID magnetometer as previously described [10]. Briefly, zero-field-cooled warming (ZFCW) and field-cooled-warming (FCW) and cooling (FCC) curves were measured between 10 and 280 K, in a field H = 8 kA/m. Magnetization *versus* applied field hysteresis loops were collected at 10 and 250 K in applied fields up to 4 MA/m.

3.4. Biological Characterization of HNPs

All tests were carried out on mouse osteoblast (7F2 cells). Cells were cultured in Alpha minimum essential media (MEM) (LifeTechnologies, UK) supplemented with 1 mM L-glutamine, 1 mM sodium pyruvate, 10% fetal bovine serum (LifeTechnologies, Paisley, UK) and 1% penicillin streptomycin.

Cell viability was estimated using trypan blue exclusion. Briefly, cells were seeded in 6-well plates (50,000/well) and cultured for 24 h. Media was removed and cells were incubated with polymer coated HNPs (6.25–100 µg mL^{-1}) diluted in fresh media for 24 and 72 h. The cells were washed three times with phosphate buffered saline (PBS) before trypsinization. Cells were resuspended in 1 mL fresh media. Cell suspension (50 µL) was mixed with 50 µL trypan blue dye (LifeTechnologies, Paisley, UK) in an Eppendorf tube and viable cells were counted on an automated cell counter (Countess™, Life Technologies, Paisley, UK). Cellular uptake was determined using cells seeded in 6-well plates (50,000/well) incubated with HNP-PEG at final concentrations of 25 µg mL^{-1} over 1,4 and 24 h. The medium was removed, and the cells washed three times with PBS, trypsinized and resuspended in 1 mL medium. The cell number was counted using the Countess™, and cells were placed in Eppendorf tubes (1×10^6 cells/tube). The cell suspensions were centrifuged at 800 rpm for 10 min, and the supernatant was removed. Concentrated hydrochloric acid (100 µL) was added to the tubes and these were incubated at 90 °C for 0.5 h. After cooling to room temperature, samples were centrifuged at 1500 rpm for 15 min. The supernatant was diluted with deionized water and run on an ICP instrument (Optima 7000V DV, PerkinElmer, Wokingham, UK). A calibration was carried out using iron standard solutions of 0.5 to 5 µg mL^{-1} ($R = 0.9999$).

The effect of the HNP-PEG on cell membrane integrity was estimated via measurement of lactate dehydrogenase (LDH) leakage from cells. Briefly, the cells were seeded in 96-well plates (15,000/well) and incubated with HNP-PEG (0–100 ug mL^{-1}) for up to 72 h. After incubation, 2 µL of lysis buffer was added to the positive control wells, and the plate was centrifuged at 1000 rpm for 5 min at 37 °C. The supernatant (50 µL) was removed from individual wells and placed into a clean plate, 50 µL of a membrane integrity assay reagent was added to the wells. The plates were incubated for 10 min at 37 °C protected from light. Stop reagent (25 µL) was then added to the wells, and the fluorescence of the samples was measured at 560 nm (excitation) and 590 nm (emission) on a microplate reader (Pro200, Tecan, Reading, UK). The percentage of cytotoxicity with respect to the positive control wells was calculated, whereby the lysed cells were assumed to have 100% LDH release.

3.5. Laser Irradiation of HNPs in Agar Phantom

HNPs (50 ug mL^{-1}) were dispersed into a 2% agar phantom in 35mm petri dishes (Greiner, UK). The samples were exposed to laser irradiation at 532 nm using a Q-switched Nd:YAG laser (10 ns pulses, 10 pulses/s). The beam was collimated in a 7 mm diameter and passed through the gel center. The temperature change was monitored using 0.076 mm diameter PFA coated T-type thermocouples (Omega, UK). One thermocouple was positioned at the center of the gel with a second placed at the edge of the gel as a control. All measurements were carried out at room temperature, 25 °C. Sample irradiation was carried out over 1 min. The temperature change in a control sample (2% agar) was measured in the absence of nanoparticles.

3.6. Incorporation of HNPs into pNiPAM Scaffolds

Samples were cut into ~1 mm thick sections using a razor blade, super critically dried and mounted onto aluminium stubs with carbon tape ready for SEM/EDXA using a bench top Hitachi TM3000 system (5 kV). For this samples were uncoated.

Field Emission Scanning Electron Microscope (FESEM, Hitachi, Japan) was conducted in a similar fashion using a Hitachi S4500 (Hitachi, Japan), coating samples with a flash of gold prior to analysis.

3.7 Laser Irradiation of pNiPAM-HNP Scaffolds

pNiPAM-HNP scaffolds were prepared into 1.5 mL Eppendorf tubes. The tubes were clamped horizontally and irradiated with a Q-switched Nd:YAG laser (10 ns pulses, 10 pulses/s) fixed at 532 nm. The beam was collimated in a 7 mm diameter and passed through the gel center. The temperature change was monitored using 0.076 mm diameter PFA coated T-type thermocouples (Omega, Manchester, UK). One thermocouple was positioned at the center of the gel. All measurements were carried out at room temperature, 25 °C. Sample irradiation was carried out over 1 min. The temperature change in a control sample (pNiPAM) was measured in the absence of nanoparticles.

3.8. Model Pharmaceutical Release

Scaffolds were prepared as previously described, with methylene blue being added into the polymer either upon formation (1 mg mL^{-1} in water solvent) or being soaked in via solvent replacement after polymerization (monolith immersed in 1 mg mL^{-1} MB aqueous solution for 2 days). To remove any surface dye which was not entrapped within the polymer scaffold, all materials were rinsed thoroughly prior to laser irradiation. Aliquots of 100 µL were taken immediately after irradiation, the polymer rinsed and retuned for repeated cycle of thermal deformation. Samples were analyzed on a Tecan M200 Pro (Tecan, UK) plate reader. Samples containing no dye were used as controls.

4. Conclusions

We have shown that when PEGylated hybrid nanoparticles are cultivated with 7F2 osteoclast cells, the toxicity is at its lowest. Particles in agar and pNiPAM-HNP composites were exposed to laser light, which resulted in localized heating of the materials. Structural alterations in pNiPAM scaffolds were brought about by ambient temperature fluctuations as well as targeted laser irradiation. Investigations into these methods for controlled release and drug integration are still ongoing.

References

1. Chrzanowski, W.; Khademhosseini, A. "Smart" materials inspired by biology. Adv. Drug Deliv. Rev. 2013, doi:10.1016/j.addr.2013.03.001.
2. Atala, A. Strategies for regenerative medicine. Surg. J. Paediat. 2012, 47, 17–28.
3. Panagiotou, N. Factors influencing medical diagnostics change. 31–34 in Clin. Chim. Acta 2013, 415.

4. Yang, Y.; Lee, L.J.; Yang, S.T.; Basu, S.; Tomasko, D.L. creation of distinct PLGA scaffolds with the use of carbon dioxide bonding and innovative microembossing. Biomaterials 26, 2585-2594, 2005.
5. Tai, H.; Mather, M.L.; Howard, D.; Wang, W.; White, L.J.; Crowe, J.A.; Morgan, S.P.; Chandra, A.; Williams, D.J.; Howdle, S.M.; et al. regulation of the structure and pore size of scaffolds for tissue engineering produced by supercritical fluid processing. Eur. Cells Mater. 14, 64–77, 2007.
6. Mohan, N.; Nair, P.D. New multisaccharide scaffolds with pores for tissue engineering uses.
2005, 18, 219–224. Trends Biomater. Artif. Org.
7. Bone Tissue Engineering: Present and Prospective Developments by A.J. Salgado, O.P. Countinho, and R.L. Reis. Biosci. Macromol. 2004, 4, 743-765.
8. Upadhyay, D.; Scalia, S.; Vogel, R.; Salama, R.O.; Young, P.M.; Traini, D.; Chrzanowski, W.

Magnetized thermoresponsive lipid vehicles for regulated and targeted lung drug delivery. 2012, 29, 2456–2467; Pharm. Res.
Hybrid gold-iron oxide nanoparticles as a multipurpose platform for biological applications (Hoskins, C.; Min, Y.; Gueorguieva, M.; McDougall, C.; Volovick, A.; Prentice, P.; Wang, Z.; Melzer, A.; Cuschieri, A.; Wang, L.). 10. Barnett, C.M.; Gueorguieva, M.; Lees, M.R.; McGarvey, D.J.; Darton, R.J.; Hoskins, C. J. Nanobiotechnol. 2012, 10, 27. 10. impact of the hybrid composition on the shape and physicochemical characteristics of gold-iron oxide nanoparticles. In 2012, J. Nanopart. Res. 14, 1170. 11. By using gold-coated iron oxide nanoparticles for improved tumor targeting with external magnetic fields, Wagstaff, A.J.; Brown, S.D.; Holden, M.R.; Craig, G.E.; Plumb, J.A.; Brown, R.E.; Schreiter, N.; Chrzanowski, W.; Wheate, N.J. Cisplatin drug delivery using gold-coated. Acta Inorg. Chim. 2012, 393, 328–333.
12. Riggio C., Hoskins C., Calatayud M.P., Pinkernelle J., Sanz B., Torres T.E., Ibarra M.R., Wang L., Keilhoff G., Goya G.F., et al. Magnetic nanoparticles coated with poly-l-lysine as intracellular neural guiding actuators. 2012, Int. J. Nanomed. 7, 1–12.
13. MR contrast agents based on iron oxide: From chemistry to cell labeling, Laurent, S.; Boutry, S.; Mahieu, I.; Vander Elst, L.; Muller, R.N. 16, 4712–4727; Curr. Med. Chem. 2009, 16.
14. Valenzueka, S.M.; Cortie, M.B.; Pissuwan, D. Gold nanoparticles heated by plasmon have potential therapeutic uses. Biotechnological Trends, 2006, 24, 62–67.
15. El-Sayed, M.A.; Jain, P.K. Cancer is the target of Au nanoparticles. 2007; Nanotoday, 2, 18–29.
16. Chan, A.; Roach, P.; Orme, R.P.; Fricker, R.A. Stimulus-responsive materials may be controlled locally or remotely for therapeutic administration. Drug Delivery Advances, 2012, in press.
17. Biodegradable synthetic polymers: Synthesis, functionalization, and biomedical applications (Tian, H.; Tang, Z.; Zhuang, X.; Chen, X.; Jing, X.). 237–280 in Prog. Polym. Sci. 2012, 37.

18. Plunkett, K.N.; Zhu, X.; Moore, J.S.; Leckband, D.E. PNIPAM chain collapse is dependent on the grafting density and molecular weight. Langmuir 2006, 22, 4259–4266.
19. Dimitrov, I.; Trzebika, B.; Müller, A.H.E.; Dworak, A.; Tsvetanov, C.B. Water-soluble copolymers that are thermosensitive and have doubly responsive reversibly interacting entities. Science Prog. 2007, 32, 1275–1343.
20. Thermoresponsive colloids in cancer treatment Abulateefah, S.R.; Spain, S.G.; Aylott, J.W.; Chan, W.; Garnett, M.C.; Alexander, C. 2011, 11, 1722–1734; Macromol. Biosci.